Wind Effects on Smoldering Behavior of Simulated Wildland Fuels

Jeanette Cobian-Iñiguez [a*], Franz Richter[b], Luca Carmignani [b], Christina Liveretou [b], Hanyu Xiong [b,c], Scott Stephens[d], Mark Finney[e], Michael Gollner[b], Carlos Fernandez-Pello[b].

[a]Department of Mechanical Engineering, University of California, Merced, USA; [b]Department of Mechanical Engineering, University of California, Berkeley, USA;[c]Department of Fire Safety Engineering, University of Science and Technology, China; [d]Department of Environmental Science, Policy and Management, University of California, Berkeley, USA; [e]Missoula Fire Sciences Laboratory, Rocky Mountain Research Station, US Forest Service, Missoula, Montana, USA

[*]Corresponding Author Email: jcobian3@ucmerced.edu

Wind Effects on Smoldering Behavior of Simulated Wildland Fuels

The current study presents a series of experiments investigating the smoldering behavior of woody fuel arrays at various porosities under the influence of wind. Wildland fuels are simulated using wooden cribs burned inside a bench scale wind tunnel. Smoldering behavior was characterized using measurements of both mass loss and emissions. Results showed that the mean burning rate increased with wind speed for all cases. In high porosity cases, increases in burning rate between 18% and 54 % were observed as wind speed increased. For low porosity cases an increase of about 170% in burning rate was observed between 0.5 and 0.75 m/s. The ratio of CO/CO_2 emissions decreased with wind speed. Thus, wind likely served to promote smoldering combustion as indicated by the decrease of CO/CO_2 which is a marker of combustion efficiency. A theoretical analysis was conducted to assess the exponential decay behavior in the time-resolved mass loss data. Mass and heat transfer models were applied to assess whether oxygen supply or heat losses can solely explain the observed exponential decay. The analysis showed that neither mass transfer nor heat transfer alone can explain the exponential decay, but likely a combination thereof is needed.

Keywords: wildfires; smoldering; cribs; bench scale

Introduction

Wildfire activity around the globe has increased in recent years within many different regions and ecosystems. Driving this increase are a variety of factors, including fire exclusion (suppression), land use changes, and climate change (Abatzoglou and Williams, 2016). More often than not, these factors compound, such as in the case of forests experiencing fuel regime shifts driven by climate factors (*e.g.* Hess *et al.*, 2019). In regions undergoing massive tree mortality, the forest floor may undergo a shift in composition from thin fuels to large woody fuels. One such instance is the accelerated tree mortality in the Sierra Nevada range, a mountain range spanning through the central valley and eastern portions of California, which has led to the rapid accumulation of large diameter downed fuels on the forest floor (Stephens *et al.*, 2018). The presence of these fuels represents a shift in surface fuel layer composition; from thin fuels such as grasses and debris which burn quickly in the flaming regime, to large, downed trees that burn over long durations in the smoldering regime. With the shift to large fuels which experience significant post-frontal smolder combustion, a new challenge arises for operational fire models that generally assume fuel beds are homogeneous and that fires spread through thin fuels in a flaming regime (Rothermel, 1972). Even for those models which characterize fuel consumption for long-term fuel burning (Albini, 1976; Albini and Reinhardt, 1995, 1997), the influence of external winds is absent. To meet this challenge, a more comprehensive understanding of the smoldering behavior of large woody wildland fuels is required.

Smoldering fires which burn in the solid, rather than gas phase, are characterized by longer burning periods and lower temperatures, heat release and spread rates than flaming fires; moreover, smoldering combustion is an incomplete mode of combustion exhibiting higher CO/CO_2 ratios than flaming combustion (Rein, 2016). Furthermore, it has been shown that smoldering fires, require lower heat fluxes to ignite than flaming fires (Boonmee and Quintiere, 2002). Because smoldering fires require less energy to ignite, the transition from smoldering to flaming is often considered a shortcut to flaming ignition (Santoso *et al.*, 2019). Most models of wildfire spread assume that a fire primarily burns as the flaming front passes unburned fuels (see Frandsen 1971; Rothermel 1972). This is true for thin wildland fuels; however, for large woody fuels, a significant portion of burning may take place in the form of smoldering after the flaming front has passed (Keane *et al.*, 2020).

A large number of previous studies on smoldering of woody fuels have focused on peat fires (*e.g.* Rein et al. 2008, Huang et al. 2016, Pastor et al. 2017, Huang et al.

2017, Davies et al. 2013, Palamba et al. 2017, Yang et al. 2016, 2019; Frandsen et al 1991). Peat is a porous and relatively homogeneous fuel compared to the large woody wildland fuels that are better described as a porous system made up of individual porous fuel elements. Although peat fires are structurally different than large woody fuels, lessons learned from studying fire behavior in peat highlight important features of smoldering fire behavior. For instance, Huang *et al.* (2016) and Rein *et al.* (2017) showed that wind increases spread rate and oxygen supply in smoldering peat fires, whereas Huang *et al.* (2016), identified increases in heat release rate in the presence of external wind. In addition to peat, other natural smoldering fuels have also been investigated. In a study of cotton bales (Xie *et al.*, 2020) wind was observed to enhance spread rate and to promote smoldering to flaming transition.

Ohlemiller (1991) examined the effects of wind on smoldering spread and transition to flaming in solid wood channels constructed from red oak and white pine. Notably, the intended application of his work were fires occurring in the built environment. Their experiments examined smoldering spread under the influence of wind speeds in the range of 0.8 to 2.2 m/s. At the lowest wind speeds examined smoldering combustion successfully propagated until the point of extinction whereas at the highest wind speeds, smoldering to flaming transition was likely to occur.

Wood cribs have long been used as a canonical configuration to model both the steady burning behaviour of fires (Gross, 1962) in structures and the spread of wildland fires. Foundational work by Fons *et al.* (1963), Byram (1964) and a collection of work led by Thomas (1964, 1965, 1967, 1971) contributed to our understanding of wildland fire spread, some of which was built upon by Rothermel (1977) in his widely used model for fire spread. Although previous work using wooden cribs occasionally addressed wind, (Thomas, 1965), this work primarily focused on wind's effect on fire spread in the flaming regime – not steady burning or its effects on smoldering combustion.

McAllister and Finney (2016) more recently extended past work on wooden cribs and applied it to understanding burning rates during flaming combustion of wooden cribs incorporating different geometries under wind. The results showed correlations with classical flaming burning rate models including those by Gross (1962) and Heskestad (1973), who first defined a crib porosity parameter, which is function of the crib geometry (2016, 2019). Their study showed the effect of wind, fuel bed porosity and crib stick width to length ratio on flaming burning rate. For densely-packed cribs under the influence of wind for instance, burning rate increases of up to 69.9% were observed as wind speed was increased (2016).

The Burnup model (Albini, 1976; Albini and Reinhardt, 1995, 1997) is perhaps the best known of the burning rate models for wildland fuels. The burning rate model in Burnup, resulting from a heat balance between the rate at which fuel reaches a critical burning temperature and the rate of heat transfer, was developed under the assumptions of flaming fires in still air. A recent review by Hyde *et al.* (2011) highlights works on coarse woody debris (Rostami, Murthy and Hajaligol, 2004; Souza and Sandberg, 2004); however, something currently missing in the literature is a delineation of the smoldering burning rate behavior in woody fuels under the presence of wind. Knowledge of such behavior could help advance fundamental understanding of smoldering fire behavior in large woody fuel beds in the wildland.

In this study we aim to fill voids in understanding of smoldering burning behavior of woody wildland fuel beds by approximating them as wood cribs. Wood cribs have been widely used in the study of structural fires because they provide a means to control the void fraction and geometrical arrangement of the fuel elements.

Similarly, they can be used to describe a wildland fuel bed in a controlled geometrical arrangement that approximately mimics that of real large wildland fuels and permits the systematic variation of the fuel bed porosity and fuel load characteristics. Thus, we focus on quantifying the smoldering burning rate of wooden fuels at various porosities under the influence of wind. To this end, a series of experiments were conducted in a bench scale wind tunnel where fuel beds were simulated using wooden cribs of different porosity.

Materials and Methods

The experimental approach was to burn wood cribs that simulated wildland fuel beds in a bench scale wind tunnel with a focus on the smoldering, post-flaming combustion regime. A schematic of the experimental apparatus is shown in Figure 1. The apparatus consists of a bench scale wind tunnel with a test section where the fuel bed is mounted on a platform attached to a load cell located outside of the tunnel. The tunnel test section is 55 cm long with a 13 cm by 8 cm cross section with windows on the sides for optical access. In a similar approach to that in McAllister (2019) porous wildland fuel beds were modeled using small wooden cribs with different porosities. Thus, cribs represented a porous fuel bed. The cribs were formed with square cross-section wooden sticks fabricated from commercially available poplar dowels. It is worth noting that in this study, the porous system of focus is the fuel bed not the wood; thus, wooden stick density variations are not considered.

Dowels were prepared for crib construction by cutting them to size with a saw, deburring edges with a carbon steel flat file, and drying them at 105 ^{o}C for at least 24 hours. The moisture content (MC) was measured after removing the dowel pieces from the oven using a moisture analyzer to ensure a moisture content of less than 1%. To construct the cribs, the wooden sticks were stacked in multiple layers with each layer oriented perpendicularly to the adjacent layers. No adhesives or nails were used. The crib porosity was calculated by using formulations first proposed by Gross (1962), and later refined by Heskestad (1973). Porosity, φ, as defined by Heskestad (1973) is a function of stick placement within the crib and is defined by,

$$\varphi = s^{\frac{1}{2}} b^{\frac{1}{2}} \left(\frac{A_v}{A_s}\right) \tag{1}$$

where s is spacing and A_v and A_s correspond to the area of the vertical shafts in the crib and exposed stick surface area respectively, and are defined by,

$$A_s = 4blNn\left[1 - \frac{b}{2l}\left(n - 1 - \frac{n}{N}\right)\right] \tag{2}$$

$$A_v = (l - nb)^2 \tag{3}$$

Equations (2) and (3) correspond to original equations by Gross (1962) reformulated by Croce and Xin (2005), where b is the stick thickness, n is the number of sticks per layer, l is stick length, and N is the number of layers. Three porosity values were chosen for this study based on keeping the initial mass of the crib constant and the geometry determined by the thickness of the sticks; a summary of the crib parameters is presented in Table 1. Notably, porosity acts here as a proxy for both the void fraction and permeability of the system. The permeability of the wooden cribs is on the order of mega-Darcy which means the fuel beds are very permeable. The porosity was estimated at the beginning of the experiments, as a change in porosity was observed in some experiments. To obtain instantaneous mass readings, cribs were placed on a false floor of the wind tunnel test section which is secured to the top of the load cell. Compressed dry air was flowed through the wind tunnel at calibrated centerline velocities equal to 0.5 m/s, 0.75 m/s, 1 m/s, and 1.25 m/s at the leading edge of the fuel for all tests. At several times during the test campaign the velocity was also measured along the vertical and longitudinal axes of the test section to assess uniformity of the flow, with variations of less than 10% found. It should be noted that these flow velocities are near the fuel bed surface and consequently correspond to significantly higher air velocities at tree canopy level (Albini, 1979). The air flow velocity is one of several parameters affecting the crib smoldering process; it affects the rate of oxygen supply to the surface of the fuel but also cools down the wood, thus affecting the rate of smoldering within the crib. To understand the effect of crib design on fire behavior, three crib configurations corresponding to low, medium, and high porosity were used. Non-dimensional porosities for the low, medium, and high porosity cribs, as calculated by Equation (1) were 0.002, 0.043 and 0.296, respectively. Table 1 summarizes the geometric properties for each crib configuration. Each crib configuration was burned under the four different wind speeds, thus resulting in 12 experimental combinations. Each experiment was repeated at least three times for a total of 61 individual experiments.

The cribs were ignited in the flaming regime and allowed to naturally transition to smoldering, mimicking conditions that would occur as a flaming fire front moves over large woody fuels and a post-fire smoldering bed remains. Specifically, the cribs were ignited by soaking them in alcohol (5 ml) and igniting the alcohol with a propane torch. Flames would spread throughout the crib and eventually the fire would transition to a smoldering state. The moment of transition was recorded as the time at which the last flame was visually present over the dowels. Experiment videos recorded at 30 frames per second, obtained using a camera oriented through a side-view window of the wind tunnel test section, were used to confirm the time of the full transition from flaming to smoldering. During flaming combustion, the lid of the wind tunnel was kept open and there was no forced airflow in the wind tunnel, limiting emissions measurements described below during the flaming regime. The wind tunnel was then closed, and the air was switched on after the transition to smoldering (an air flow before a full transition could have caused reignition of the fuel bed into a flaming mode). It is worth noting that the experiment was not initially designed to examine the mechanisms producing flaming to smoldering transition, with flaming combustion was only used as a means to initiate smoldering combustion.

The emissions of combustion products were monitored using an ENERAC 700 emissions analyzer. The ENERAC 700 captures CO, NO, NO_2, SO_2 and Hydrocarbons; the device includes a moisture condenser which prevents condensation in the sampling tube. Sampling was conducted downstream from the crib by inserting the sampling probe by the exhaust duct of the wind tunnel. The probe was placed along the midplane of the wind tunnel (see Figure 1). Sampling was conducted at 1 Hz. During the flaming portion of every experiment, when the wind tunnel was open and the wind was off, emissions built up along the length of the tunnel, which were all flushed out at once when the wind was switched on after the smoldering transition. For this reason, the emissions data was considered to be supplemental information, while the primary data (mass variation) was recorded by the scale.

The mass was measured using the Radwag PS 1000.R1 precision balance with a readability of 0.001g which is useful for capturing precise measurements near the end of the smoldering phase. The mass of the crib was measured for the entire duration of the experiment (both flaming and smoldering phases). The load cell was connected to a computer where all of the data, sampled at a rate of 240 Hz, were saved automatically. The mass data were then analyzed to find the burning rate for experiments of different porosities and wind speeds. Each crib configuration (low, medium and high porosity) was burned under the four different wind speeds indicated by Table 1 thus resulting in 12 experimental combinations.

Results

The experiments presented here followed the typical sequence depicted by Figure 2. There it can be seen that, upon ignition, the initially alcohol-soaked crib was allowed to become fully engulfed by flames. During the flaming portion of combustion, the overall crib structure typically remained stable with the exception of individual sticks experiencing deformation; in some instances, sticks would fall off the main structure, likely due to stick deformation, reduced density, and both ambient and fire-induced winds. As the flame receded and combustion transitioned to the smoldering regime, the sticks continued to burn and depending on the crib design, some cribs collapsed from the center as smoldering combustion progressed.

Figure 3 shows the variation of the crib mass in time, as well as the relative mass loss rate, for a representative experiment conducted under a 0.75 m/s wind speed using a crib with medium porosity (see Table 1). The initial mass of the crib in the smoldering phase is about 6 g; the mass is halved in the first 200 s of the experiments, and then it takes about 400 s to further reduce the final mass value. The mass loss rate decreases in time in a similar fashion, decreasing more than five times in the first 200 s of the smoldering phase.

Figure 4 shows the raw mass loss data from the experiments as function of wind speed (columns) and porosity (rows). Even under the same conditions, repeated experiments often start with different initial masses and the burning times, thus it is difficult to compare the results from different tests. Nevertheless, all experiments seem to follow the same general pattern. They start at a relatively high initial mass at the end of the flaming ignition period and then decay to lower final mass (see Figure 4). The rate of decay slows as time goes on. This indicates that after the flaming ignition transition into smoldering, the smolder burning rate decays toward a semi-constant value. As it was pointed out above, the flaming ignition of the fuel followed by the transition to smolder, represents the event that would occur after the passage of a frontal burning wildfire (post-frontal smolder combustion). Thus, this smolder rate decay is expected to occur after the passage of the wildland flaming fire front leading to a semi-steady, or residual smolder (Rein 2016) with a burning rate determined by the characteristics of the woody fuel bed and the environment.

We normalized the experimental data to facilitate the comparison between the different tests which reveal that this pattern takes place in all the tests and is represented by an exponential decay as shown in Figure 5. The mass loss and time were normalized as

$$m^* = \frac{m(t) - m_f}{m_i - m_f} \tag{4}$$

and

$$t^* = \frac{t}{t_f} \tag{5}$$

where m^* is the normalized mass, m_f is the final residual mass at the end of the experiment, m_i is the initial mass at time 0, $m(t)$ is the mass, t^* is the normalized time, t is time in seconds and t_f is the final time. We were then able to fit to all data an exponential decay in the form of Eq. (6) with an R^2 value of over 0.96 for each experiment. We only removed one extreme outlier at a windspeed of 0.5 and medium porosity. The normalized mass was then fit as an exponential function,

$$m^* = \exp(-\lambda t^*) \tag{6}$$

where λ is the exponential decay constant.

The exponential decay was obtained using a burning rate function derived from the half-life via Eq. (7).

$$\dot{m}_{0.5} = \frac{m_i - m_f}{t_f}\frac{0.5}{t_{0.5}^*} = \frac{m_i - m_f}{t_f}\frac{0.5\lambda}{\ln 2}, \tag{7}$$

where $\dot{m}_{0.5}$ is the burning rate based on half-life and $t_{0.5}^*$ is half-life.

Figure 6 shows the burning rate for each experimental configuration, with the relative values reported in Table 3. The mean for all experiments in each experimental configuration is represented by a dot. Colors represent porosity and the dot size denotes mean mass loss rate (g/s) with a larger dot corresponding to a greater mass loss rate. Mean mass loss rate is presented in this plot as a function of wind speed and porosity, where porosity is on the y-axis, therefore all dots at a particular y location are the same color; wind speed is presented on the x-axis. This arrangement allows for visualization of the effect of wind speed and porosity on burning rate. As can be seen in the figure (and from the values listed in Table 3), high porosity experiments exhibited a gradual and substantial increase in burning rate with wind speed. For these cases, the burning rate increased by 45% between 0.5 m/s and 0.75 m/s, by 18% between 0.75 m/s and 1 m/s and by 54% between 1 m/s and 1.25 m/s. In the case of the low and medium porosity experiments, there is a more modest increase in burning rate with respect to wind. The low porosity cribs show a much larger increase in burning rate from 0.5 to 1 m/s (about 170%) compared to the case of the medium cribs (about 41%), but they both show very little variation above 1 m/s (7% and 4%, respectively, for low and medium porosity cribs). This slight increase in burning rate with the porosity could be a result of enhanced burning efficiency as oxygen has easier access to the reaction side, and products are transported away. More intense visible glowing during the experiments provides additional evidence for this hypothesis.

To assess completeness of combustion, a CO/CO_2 ratio was obtained for each experiment. Only results for the smoldering combustion are presented. The time dependent CO/CO_2 emissions data were averaged for each experiment to obtain average CO/CO_2 ratio for each experimental configuration. The average smoldering combustion emissions for all experiments for each wind speed is presented in Figure 7. The different colors in the plot represent the crib porosity values (low, medium, high). Despite the large standard deviation between the data points, which is something relatively common for realistic smoldering investigations (Hakes *et al.*, 2019), some observations can be made. Trendlines were fitted across experiments of equal porosities in order to understand the effect of wind speed. With this approach it was observed that, in general, CO/CO_2 emissions decreased with wind speed. Furthermore, for wind speeds of 0.5 m/s, 0.75 m/s and 1.25 m/s, the mean CO/CO_2 ratio increased with porosity. The greatest increase in mean CO/CO_2 ratio with respect to porosity occurred for the lowest wind speed, 0.5 m/s.

Theoretical Analysis

We will concentrate here on deriving a physical explanation for the exponential decay of the mass loss rates observed in the experiments reported in the previous section. The analysis describes the decay in the smolder rate that would be expected to occur after the passage of the wildfire flaming front.

Ohlemiller (1985) argued that smoldering systems are controlled by two physical processes: oxygen supply and heat losses. These results were derived for porous fuels, which differs from our novel experimental set-up that resembles a porous system with porous fuels within. Concerning the controlling mechanism proposed by Ohlemiller (1985) the two physical processes are related, since the oxygen supply will determine in part the burning and heat release rate, and the heat losses the balance of energy that sustains the smolder burning. In this section, we will test the hypothesis that the interplay between the oxygen supply and the heat losses can explain the observed exponential decay. If a process is controlled by oxygen supply, which means the rate of reaction is limited by the supply of oxygen, then we will call the process mass transfer controlled/limited. If a process is controlled by heat losses, which means the rate of reaction is limited by the temperature at the reaction front, then we will call the process heat transfer controlled/limited. To this end, we will first derive a simple analytical model for oxygen supply followed by a simple model for heat losses.

For the first case, a mass transfer, or shrinking-core, model, we will assume that if the burning of a single stick in the crib is mass limited then the process of the whole crib burning is limited. To this end, we will approximate a single wooden stick as a porous cylinder (called a pellet) in which the grains are also of cylindrical shape (called grains). This set-up allows us then to use the shrinking-core model by Sohn and Szekely (1972). To use their model, we implicitly assume that smoldering takes place only at the surface of the grains, that diffusion mass transfer within the pellet is limiting, and that the reaction rate is fast compared to mass transfer (Froment, Bishoff and De Wilde, 2011). These assumptions allowed Sohn and Szekely to derive Eqs. (8-10),

$$t_{norm} = 1 - (1-\alpha)^{0.5} + \sigma^2\left(\alpha + (1-\alpha)\, ln(1-\alpha) + \frac{2\alpha}{N_{sh}}\right), \tag{8}$$

where α is called conversion and defined in Eq. (9)

$$\alpha = 1 - m^* \tag{9}$$

and t_{norm} is the normalized mass that can be converted to t^{**} using Eq. (10)

$$t^{**} = \frac{t_{norm}}{t_{norm}(\alpha = 1)}. \tag{10}$$

The parameter σ is a function of the surface areas and volume of the grain and pellet, the rate constant, the diffusion coefficient, and porosity. The parameter N_{sh} is the modified Sherwood number, which is assumed to be equal to three. Further details on the derivation, their assumptions, and limitations can be found in Sohn and Szekely (1972) and Froment, Bishoff and De Wilde (2011).

In Figure 8, we present a comparison between the experimental results and the shrinking-core model (Eq. (8) – (10)) with the two limiting cases of $\sigma \to 0$ and $\sigma \to \infty$. The figure shows that the shrinking-core model is able to reproduce the exponential trend but cannot quantitatively capture the smoldering behavior of the crib. In fact, the experimental data lie outside the theoretical limit—that is the experimental curves are on the left of the shrinking-core model with $\sigma \to \infty$, which suggests that mass transfer alone does not control this smoldering process.

The second hypothesis we tested is that heat losses control the decay parameters. The underlying physical explanation is that we had a strong ignition that is followed by weak smoldering. This means that the smoldering isn't self-sustained and feeds from the residual heat of the ignition process. To test this hypothesis, we made the following 6 assumptions:

(1) Each stick burns individually and can be modelled as a cylinder of char.

(2) The rod can be assumed to be at a uniform temperature throughout (lumped capacitance assumption)

(3) The rod burns uniformly with $r \to 0$ and $l = constant$

(4) No heat is generated, as generation of heat during smolder is small compared to the loss of heat to the surrounding.

(5) The shrinking rate (dr/dt) is controlled by a one-step chemical kinetic reaction

(6) Mass transfer is infinitely fast

These assumptions lead us to effectively model a cooling shrinking cylinder. We can write that the change in thermal energy in the cylinder is given by Eq. (11),

$$\frac{dQ}{dt} = c_p m \frac{dT}{dt} = c_p \rho \pi l \, r^2 \frac{dT}{dt}. \tag{11}$$

where Q is the thermal energy, c_p the heat capacity, l the length of the cylinder, r is the current radius of the cylinder, and T the temperature of the cylinder.

The heat losses are then given by Eq. (12).

$$\frac{dQ}{dt} = -hA\,\Delta T = -h2\pi lr\,\Delta T\,\left(1 + \frac{r}{l}\right) \tag{12}$$

where h is the convective heat transfer coefficient adjusted for radiation, A is the surface area of the cylinder, and ΔT the temperature difference between the cylinder and environment.

We can then equate Eq. (11) and (12) to get Eq. (13)

$$\frac{dT}{dt} = -\frac{2h}{\rho c_p R}\left(1 + \frac{1}{\iota}\frac{r}{R}\right)\frac{1}{\left(\frac{r}{R}\right)}\,\Delta T \tag{13}$$

where ι is the aspect ratio, R is the initial radius, and $\Delta T = T - T_a$ with T_a being the ambient temperature. Introducing a new variable α given by Eq. (14),

$$\alpha = 1 - \left(\frac{r}{R}\right)^2 \tag{14}$$

we can then define the shrinking of cylinder by Eq. (15) and express the whole equation in terms of r using Eq. (14).

$$\frac{dr}{dt} = -\eta(1-\alpha) = -\eta\,\left(\frac{r}{R}\right)^2 = -A\,exp\left(-\frac{E}{R_u T}\right)\left(\frac{r}{R}\right)^2 \tag{15}$$

Where η is the rate constant, A the pre-exponential factor, E the activation energy, and R_u the universal gas constant. Eq. (15) can be expressed completely in terms of r/R by multiplying both sides by 1/R to get Eq. (16).

$$\frac{d\left(\frac{r}{R}\right)}{dt} = -\frac{A}{R}\, exp\left(-\frac{E}{R_u T}\right)\left(\frac{r}{R}\right)^2 \tag{16}$$

After solving Eq. (13) and (16) numerically, we normalized the time following Eq. (5). The parameters used are given in Table 2, but we found that after the normalization of time the choice of parameters has an insignificant influence on the result.

Figure 8 illustrates the comparison between the heat transfer model (Eq. (13) and Eq. (16) with the experimental data and the mass transfer model (Eq. (8)). Just as the mass transfer model, the heat transfer model can reproduce the exponential trend. In fact, the two models encapsulate most of the experimental data. This encapsulation suggests that the experiments are a result of the interplay between mass transfer and heat losses as predicted by Ohlemiller (1985). Neither mass transfer nor heat transfer alone can explain the exponential decay, but likely a combination thereof is needed. One limitation of the heat transfer model is that it never fully converts to $\alpha = 1$ as the heat losses cause the reaction to slow down to much as $\alpha \rightarrow 1$. We were, therefore forced to normalize the curve to $t(\alpha = 0.98)$.

Discussion

At first glance, the theoretical results appear trivial as they have been shown previously for other smoldering systems. These other smoldering system are categorized by Torero *et al.* (2020) as either a solid porous fuel (e.g., a block of wood, foam, etc) or as condensed fuels in an inert media (e.g., tar in sand) (Torero *et al.*, 2020). Our system is neither of those two, as we have a smoldering wood crib which presents a porous system (the crib) made out of a porous fuel (the wood). The system is, therefore, novel, but our analysis suggest that it can be modeled using the same tools as for traditional smoldering systems.

The mean burning rate across all experiments is presented in Figure 6, where it can be observed that, overall, the mean burning rate increased with wind speed. This increase in burning rate is likely a consequence of enhanced oxygen transport bolstering the reaction process as found for other smoldering systems (Ohlemiller, 1985; Rein, 2016). This is a general trend in all smoldering fuels, where for instance in polyurethane fuels, wind is likely to affect smoldering fire behavior through altering oxidizer supply and heat transfer to and from the fuel (Torero et al. 1993). In woody fuels, the presence of an external wind flow enhanced smoldering behavior by promoting char oxidation and heat release rate (Ohlemiller 1991). Although this effect offsets initially the increase in heat losses with wind speed, as the wind is increased further the heat losses become dominant and the smolder burning rate decreases with the wind (Torero and Fernandez-Pello, 1996)

With respect to the emissions measurements, increases in wind speed served to decrease the CO/CO_2 ratio in most cases. Being that CO/CO_2 is generally a measure of completeness of combustion, this parameter's increase with wind could be attributed to an increase in oxygen supply which acted to promote the smolder oxidation process. Further, as indicated by Rein (2013) CO_2 will typically increase with increased oxygen access while CO will decrease, thus corroborating decreases in CO/CO_2 with increased wind speed. In the case of the experimental results here, one may tie together the burning rate and emissions measurements by observing that increasing the wind speed served to promote the smolder combustion process as exhibited by the increased burning rate and decrease the CO/CO_2 ratio. Furthermore, the hydrocarbon emissions from the ENERAC 700 were analyzed to reveal that these emissions were negligible at almost all points of the experiment. The only spike in hydrocarbons was experienced right after ignition in the flaming region due to the presence of the alcohol. In the smoldering regime, the hydrocarbons were within the accuracy of the ENERAC 700, which is 4 PPM.

Summary and Conclusions

We studied the smoldering burning behavior of simulated wildland fuels through bench scale wind tunnel experiments. Woody wildland fuels were simulated using cribs which are wooden structures constructed by stacking layers of sticks. Three crib designs were tested, these corresponded to cribs with low, medium and high porosity. The effect of wind on burning behavior was tested by imposing 0.5 m/s, 0.75 m/s, 1.0 m/s and 1.25 m/s winds. Results showed that overall, the mean smolder burning rate increased with wind speed and porosity, but the latter provides a very weak trend for the present experiments. Further, the ratio of CO/CO_2 emissions decreased with wind speed. In this way, increasing the wind speed likely served to promote the smolder combustion process thus increasing the burning rate and decreasing the CO/CO_2 ratio. Analysis of time series mass data surfaced an exponential decay behavior across all experimental conditions tested. A theoretical analysis found that, although both the heat and mass transfer models reproduced the exponential decay trend, both had some limitations in completely matching the experimental data. Thus, the analysis showed that neither mass transfer nor heat transfer alone can explain the exponential decay. It is therefore proposed that instead, a combination of both mass and heat transfer could be driving the exponential decay. This result is consistent with the consensus of the literature on other smoldering systems.

It is worth noting that the results here are representative of the conditions tested. In this study, fuel uniformity was achieved by using commercially available poplar dowels, visibly free of imperfections that were oven-dried to reach a moisture content of less than 1%. Maintaining fuel uniformity allowed for increased experimental control. In this regard, we recognize that the fuels in this study are representative of idealized woody fuels and that real fuels will likely exhibit characteristics such as higher moisture contents and, in the case of downed trees, these fuels may be covered in layers of bark depending on the period of time that has progressed since tree death (Maser *et al.*, 1979). Thus, to continue advancing towards greater understanding of smoldering behavior in real woody fuels will require addition of new parameters to progressively capture the influence of fuel properties on burning behavior. Further, the scale of the cribs in this study, although of similar scale as that of surface fuels, was much smaller than that encountered in real fires, necessitating future studies with larger-diameter fuels and systems. Despite these limitations, in this study we have identified the extent to which wind and porosity affect smoldering rate in dry woody fuels, forming the basis for future experiments which may examine a wider variety of woody fuels under different moisture contents, geometries, and at larger scales. This knowledge may eventually be useful to incorporate the effect of wind on smoldering of woody fuel beds in practical models, as it is clearly shown in this work that wind effects burning rates and CO/CO_2 ratios that would influence results describing post-frontal combustion from these practical models.

The results here represent first steps in understanding the burning behavior of simulated woody fuels experiencing post-frontal, residual smolder combustion in a wildland fire. We have shown that wind speed affects burning behavior and that fuel porosity will influence the degree to which wind may enhance the burning behavior. The theoretical analysis conducted here pointed to a combustion process governed by both mass and heat transfer as well as chemical kinetics, to an extent.

Acknowledgements

The authors would like to thank Priya Garg for her assistance in implementing the emissions measurement protocol. This work was sponsored by the California Energy Commission – Energy Program Investment Charge (EPIC) program under Grant #EPC-18-026. Funding for J.Cobian came from the University of California, Merced School of Engineering.

Declaration of Interests

The authors declare no conflicts of interests.

References

Abatzoglou, J. T. and Williams, A. P. (2016) 'Impact of anthropogenic climate change on wildfire across western US forests', *Proceedings of the National Academy of Sciences*, 113(42), pp. 11770–11775. doi: 10.1073/pnas.1607171113.

Albini, F. A. (1976) 'Estimating Wildfire Behavior and Effects', *USDA Forest Service General Technical Report INT-30*.

Albini, F. A. (1979) *Estimating windspeeds for predicting wildland fire behavior*. Intermountain Forest and Range Experiment Station, Forest Service, US ….

Albini, F. A. and Reinhardt, E. D. (1995) 'Modeling Ignition And Burning Rate Of Large Woody Natural Fuels', *International Journal of Wildland Fire*, 5(2), pp. 81–91. doi: 10.1071/WF9950081.

Albini, F. A. and Reinhardt, E. D. (1997) 'Improved calibration of a large fuel burnout model', *International Journal of Wildland Fire*, 7(1), pp. 21–28. doi: 10.1071/WF9970021.

Boonmee, N. and Quintiere, J. G. (2002) 'Glowing and flaming autoignition of wood', *Proceedings of the Combustion Institute*, 29, pp. 289–296.

Byram, G. M. *et al.* (1964) *An experimental study of model fires.* SOUTHERN FOREST FIRE LAB MACON GA.

Croce, P. A. and Xin, Y. (2005) 'Scale modeling of quasi-steady wood crib fires in enclosures', *Fire Safety Journal*, 40(3), pp. 245–266. doi: 10.1016/j.firesaf.2004.12.002.

Fons, W. L., Clements, H. B. and George, P. M. (1963) 'Scale effects on propagation rate of laboratory crib fires', in *Symposium (International) on Combustion*. Elsevier, pp. 860–866.

Frandsen, W. H. (1971) 'Fire spread through porous fuels from the conservation of energy', *Combustion and Flame*, 16(1), pp. 9–16. doi: 10.1016/S0010-2180(71)80005-6.

Froment, G. F., Bishoff, K. B. and De Wilde, J. (2011) 'Chapter 4: Noncatalytic Gas-Solid Reactions', in *Chemical Reactor Analysis and Design*, pp. 240–267.

Gross, D. (1962) 'Experiments on the burning of cross piles of wood', *Journal of Research of the National Bureau of Standards, Section C: Engineering and Instrumentation*, 66C(2), p. 99. doi: 10.6028/jres.066c.010.

Hakes, R. S. P. *et al.* (2019) 'Thermal characterization of firebrand piles', *Fire safety* *journal*, 104, pp. 34–42.

Heskestad, C. (1973) ‘Modeling of enclosure fires’, *Symposium (International) on Combustion*, 14(1), pp. 1021–1030. doi: 10.1016/S0082-0784(73)80092-X.

Hess, K. A. *et al.* (2019) ‘Satellite-based assessment of grassland conversion and related fire disturbance in the Kenai Peninsula, Alaska’, *Remote Sensing*, 11(3). doi: 10.3390/rs11030283.

Huang, X. *et al.* (2016) ‘Experimental study of the formation and collapse of an overhang in the lateral spread of smouldering peat fires’, *Combustion and Flame*, 168, pp. 393–402. doi: 10.1016/j.combustflame.2016.01.017.

Hyde, J. C. *et al.* (2011) ‘The combustion of sound and rotten coarse woody debris : a review’, *International Journal of Wildland Fire*, (1972), pp. 163–174.

Keane, R. E. *et al.* (2020) ‘Drying rates of saturated masticated fuelbeds from Rocky Mountain mixed-conifer stands’, *International Journal of Wildland Fire*, 29, pp. 57–69.

McAllister, S. (2019) ‘The Role of Fuel Bed Geometry and Wind on the Burning Rate of Porous Fuels’, *Frontiers in Mechanical Engineering*, 5(April), pp. 1–9. doi: 10.3389/fmech.2019.00011.

McAllister, S. and Finney, M. (2016) ‘Burning Rates of Wood Cribs with Implications for Wildland Fires’, *Fire Technology*, 52(6), pp. 1755–1777. doi: 10.1007/s10694-015-0543-5.

Ohlemiller, T. J. (1985) ‘Modeling of smoldering combustion propagation’, *Progress in Energy and Combustion Science*, 11(4), pp. 277–310. doi: 10.1016/0360-

1285(85)90004-8.

Ohlemiller, T. J. (1991) ‘Smoldering combustion propagation on solid wood’, *Fire Safety Science: Proceedings of the Third International Symposium*, pp. 565–574. doi: 10.4324/9780203973493.

Rein, G. (2016) ‘Smoldering Combustion’, in Hurley, M. J. (ed.) *SFPE Handbook of Fire Protection Engineering*. New York, NY, pp. 581–603.

Rein, G. *et al.* (2017) ‘Detection of landmines in peat soils by controlled smouldering combustion : Experimental proof of concept of O-Revealer’, *Experimental Thermal and Fluid Science*, 88(February 2016), pp. 632–638. doi: 10.1016/j.expthermflusci.2017.07.016.

Richter, F. and Rein, G. (2020) ‘A multiscale model of wood pyrolysis in fire to study the roles of chemistry and heat transfer at the mesoscale’, *Combustion and Flame*, 216, pp. 316–325. doi: 10.1016/j.combustflame.2020.02.029.

Rostami, A., Murthy, J. and Hajaligol, M. (2004) ‘Modeling of smoldering process in a porous biomass fuel rod’, 83, pp. 1527–1536. doi: 10.1016/j.fuel.2003.11.018.

Rothermel, R. C. (1972) ‘A Mathematical Model for Predicting Fire Spread in Wildland Fuels’, *USDA For. Serv. Res. Pap. INT-115*, p. 40.

Santoso, M. A. *et al.* (2019) ‘Review of the Transition From Smouldering to Flaming Combustion in Wildfires’, *Frontiers in Mechanical Engineering*, 5(September). doi: 10.3389/fmech.2019.00049.

Sohn, H. Y. and Szekely, J. (1972) ‘A structural model for gas-solid reactions with a moving boundary-III. A general dimensionless representation of the irreversible reaction between a porous solid and a reactant gas', *Chemical Engineering Science*, 27(4), pp. 763–778. doi: 10.1016/0009-2509(72)85011-5.

Souza, F. De and Sandberg, D. (2004) 'Combustion and Flame Mathematical model of a smoldering log', *Combustion and Flame*. doi: 10.1016/j.combustttame.2004.07.009.

Stephens, S. L. *et al.* (2018) 'Drought, Tree Mortality, and Wildfire in Forests Adapted to Frequent Fire', *BioScience*, 68(2), pp. 77–88. doi: 10.1093/biosci/bix146.

Thomas, P. H. (1965) 'Fire spread in wooden cribs: Part III the effect of wind', *Fire Safety Science*, 600, p. 1.

Thomas, P. H. (1967) 'Some aspects of the growth and spread of fire in the open', *Forestry: An International Journal of Forest Research*, 40(2), pp. 139–164.

Thomas, P. H. (1971) 'Rates of spread of some wind-driven fires', *Forestry: An International Journal of Forest Research*, 44(2), pp. 155–175.

Thomas, P. H., Simms, D. L. and Wraight, H. G. (1964) 'Fire spread in wooden Cribs', *Fire Safety Science*, 537, p. 1.

Torero, J. L. *et al.* (2020) 'Processes defining smouldering combustion: Integrated review and synthesis', *Progress in Energy and Combustion Science*, 81. doi: 10.1016/j.pecs.2020.100869.

Xie, Q. *et al.* (2020) 'Smoldering Fire of High-Density Cotton', *Fire Technology*.

Table 1. Summary of crib configurations

Configuration	Stick Length (in., mm)	Stick Width (in., mm)	Sticks per Layer	Number of Layers	Porosity
Low	1.33, 33.7	0.25, 6.4	12	3	0.002
Medium	2, 50.8	0.38, 9.7	3	3	0.043
High	2.65, 67.3	0.50, 12.7	2	2	0.296

Table 2. Overview of the input parameters to the heat transfer model (Eq. (11) and (14)). The material properties are taken from the char of softwood, the geometry parameters are measured, and the kinetic parameters are taken as the kinetic parameters for the oxidation of char.

Parameter	Value	Units	Reference
ρ	361	kg/m^2	(Richter and Rein, 2020)
h	20	W/m^2-K	Assumed
c_p	2300	J/kg-K	(Richter and Rein, 2020)
ι	5.3	-	Measured
R	0.01	M	Rounded average stick width
$\log A$	9.75	log 1/s	(Richter and Rein, 2020)
E	1600	kJ/mol	(Richter and Rein, 2020)
T_a	300	K	(Richter and Rein, 2020)

Table 3. Average burning rate values shown in Fig. 5, as function of wind speed and crib porosity.

Wind speed (m/s)	Porosity	Burning rate (g/s)	Standard deviation (g/s)
0.5	0.002 (low)	0.00586	0.00385

0.5	0.043 (medium)	0.00908	0.0037
0.5	0.296 (high)	0.00456	0.000614
0.75	0.002 (low)	0.0129	0.00485
0.75	0.043 (medium)	0.00963	0.00507
0.75	0.296 (high)	0.00659	0.00126
1	0.002 (low)	0.0162	0.00941
1	0.043 (medium)	0.0121	0.00426
1	0.296 (high)	0.00779	0.00156
1.25	0.002 (low)	0.0174	0.00499
1.25	0.043 (medium)	0.0126	0.00182
1.25	0.296 (high)	0.012	0

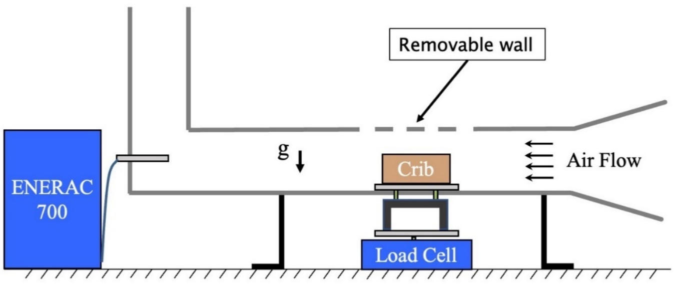

Figure 1 Schematic of experimental apparatus.

Figure 2 Evolution of a typical burn where 1) is the pre-burn period, 2) is the flaming combustion period, 3) is the smoldering period and, 4) is near the end of the experiment.

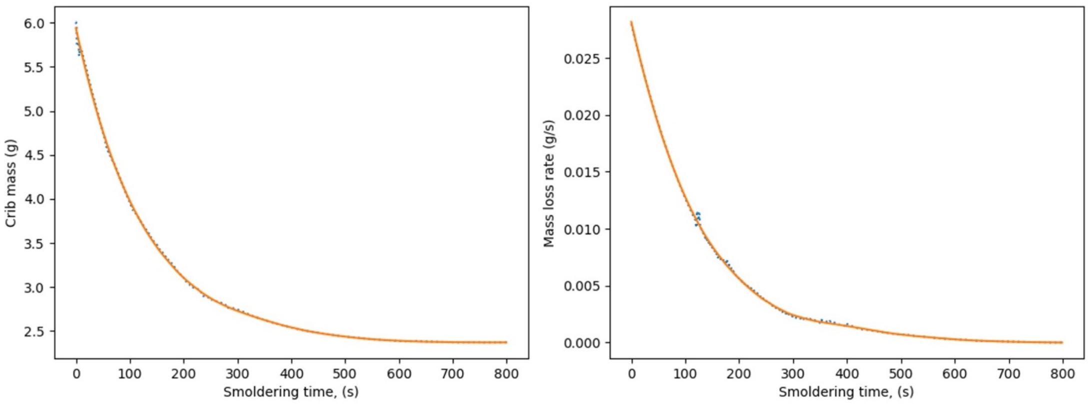

Figure 32 Representative results for a smoldering crib exposed to a wind speed of 0.75 m/s (and medium porosity) in terms of mass (left) and mass loss rate (right) variations in time. The raw data (blue dots) are smoothed to obtain the orange lines.

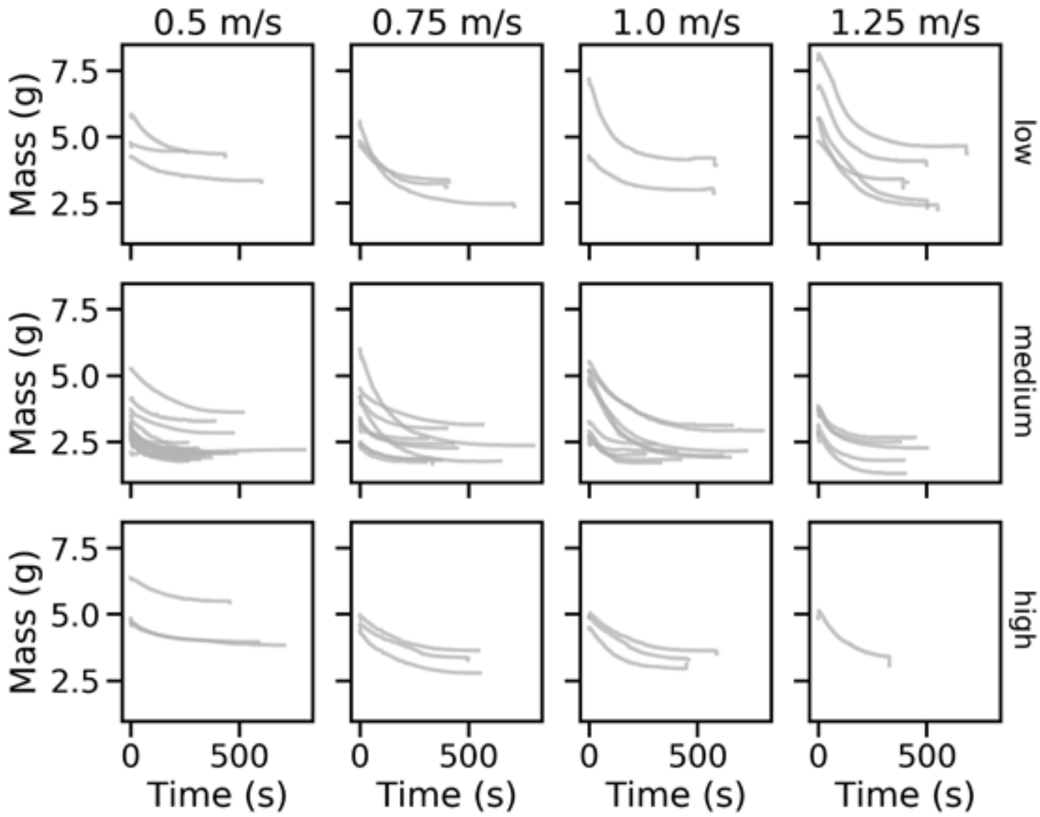

Figure 4 Overview of the mass loss in the smoldering region at four windspeeds (columns) and three porosities (rows). The data are raw (no smoothing), and the times reset to 0 to start at the beginning of smoldering. The start of smoldering was observed visually in the experiments.

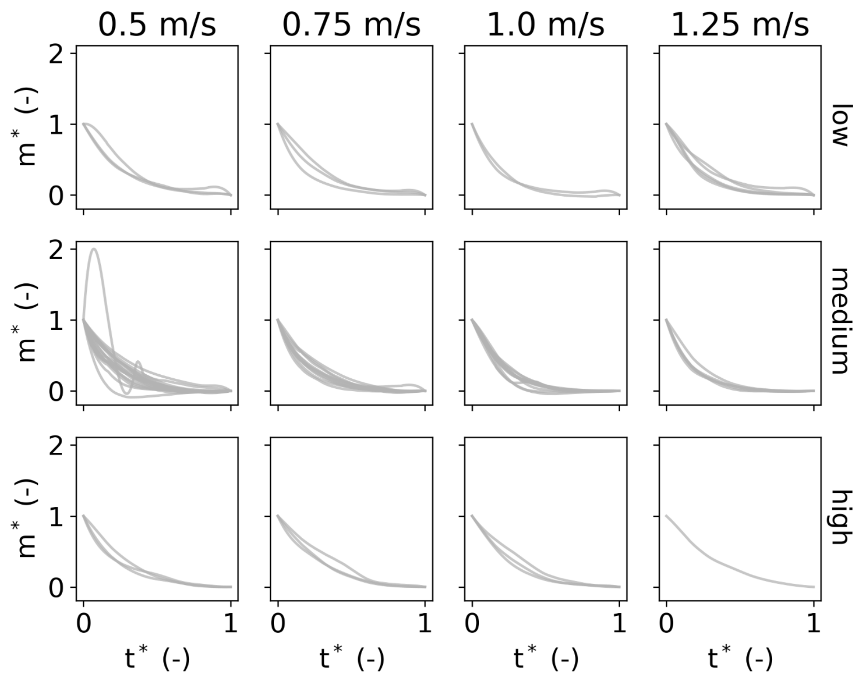

Figure 5 Overview of the raw data normalized with respect to the experimental time and total mass loss. The data show an exponential decay after the normalization. Each column represents one windspeed and each row represents one porosity.

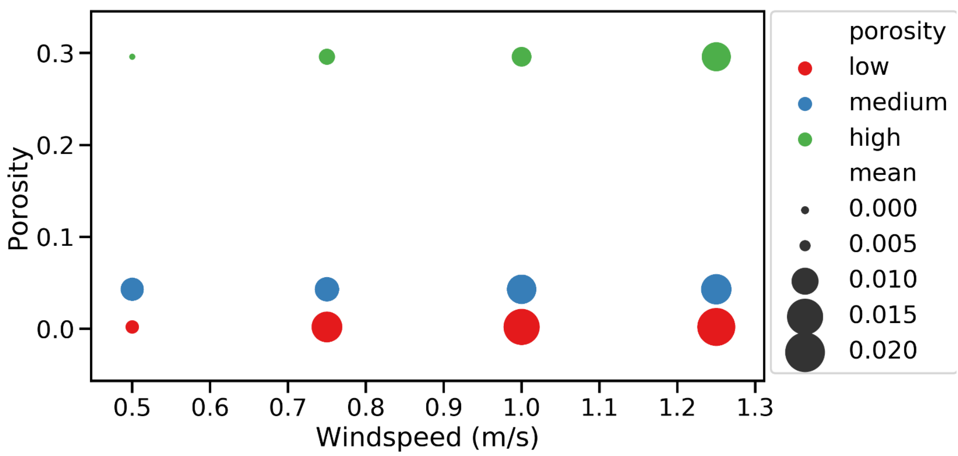

Figure 6 Average mass loss rate by varying porosity and wind speed.

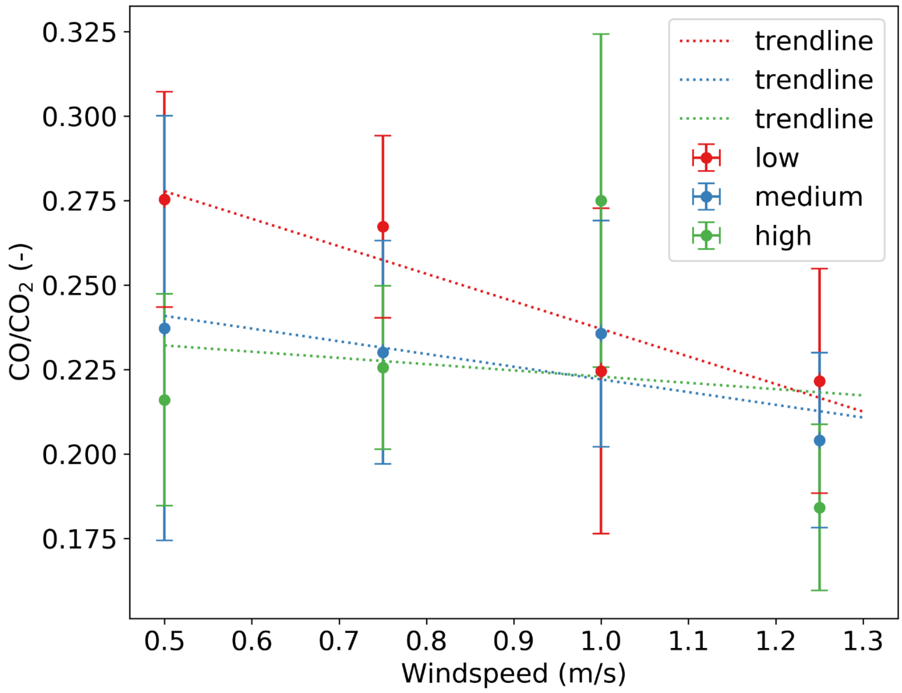

Figure 7 Average CO/CO2 measured with the ENERAC 700 during the smoldering phase of the cribs.

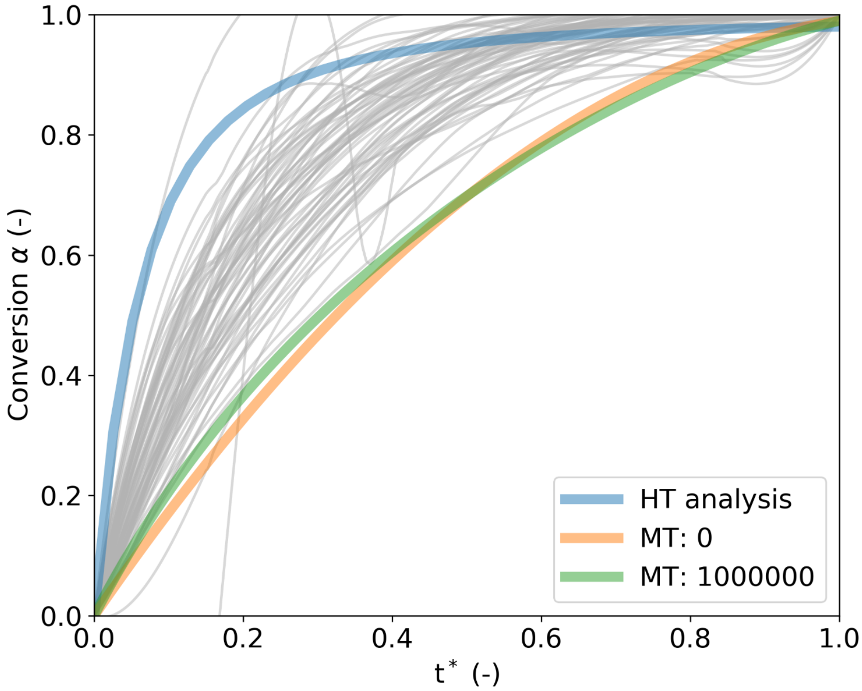

Figure 8 Comparison between the experimental results and the two derived models for heat transfer and mass transfer respectively. HT stands for heat transfer model which is the numerical solution of Eqn. 11 and 14. MT stands for the mass transfer model which is Eqn. 5, and the number behind (0 and 10^6) are the values of σ.